Nanoscale

PAPER

View Article Online
View Journal | View Issue

Cite this: *Nanoscale*, 2014, **6**, 15203

Nanoconfinement of pyrene in mesostructured silica nanoparticles for trace detection of TNT in the aqueous phase†

Pinar Beyazkilic,[a,b] Adem Yildirim[a,b] and Mehmet Bayindir*[a,b,c]

Received 21st September 2014,
Accepted 18th October 2014

DOI: 10.1039/c4nr05514d

www.rsc.org/nanoscale

This article describes the preparation of pyrene confined mesostructured silica nanoparticles for the trace detection of trinitrotoluene (TNT) in the aqueous phase. Pyrene confined mesostructured silica nanoparticles were prepared using a facile one-pot method where pyrene molecules were first encapsulated in the hydrophobic parts of cetyltrimethylammonium micelles and then silica polymerized around these micelles. The resulting hybrid particles have sizes of around 75 nm with fairly good size distribution. Also, they are highly dispersible and colloidally stable in water. More importantly, they exhibit bright and highly stable pyrene excimer emission. We demonstrated that excimer emission of the particles exhibits a rapid, sensitive and visual quenching response against TNT. The detection limit for TNT was determined to be 12 nM. Furthermore, excimer emission of pyrene shows significantly high selectivity for TNT.

Introduction

Contamination of water resources by nitroaromatic explosives, particularly trinitrotoluene (TNT), is a major global concern because these molecules are highly toxic to biological organisms.[1,2] Therefore, sensitive and selective detection of nitroaromatic explosives in water has attracted a great deal of interest in recent years.[3,4] Currently employed methods for their detection include ion mobility spectroscopy (IMS), mass spectrometry, gas chromatography (GC), and infrared absorption spectroscopy.[4,5–8] Although these methods are usually sensitive, development of simple and handheld techniques such as fluorescence based systems (consisting of a simple UV lamp and a fluorescent probe) has attracted a great deal of interest due to their portability and ease of use. For instance, using quantum dots,[9–11] fluorescent dyes,[12–14] metal organic frameworks (MOFs),[15–17] and conjugated polymers,[18–21] nitroaromatic molecules were detected in the aqueous phase. However, these methods generally have some drawbacks such as high detection limit, interference from non-nitroaromatic compounds, laborious and costly synthesis and poor stability of fluorescent probes under the atmospheric conditions. Therefore, facile and cost-effective development of robust nitro-explosive sensing platforms with good sensitivity and selectivity is still needed.

In this context, we report the preparation of pyrene confined mesostructured silica nanoparticles for rapid and reliable detection of TNT in water. It is well known that fluorescence of pyrene (a π-conjugated fluorophore with high quantum yield and long lifetime) is quenched by nitroaromatic explosives through photoinduced electron transfer (PET).[22,23] Particularly, excimer emission of pyrene, which is observed in the presence of π–π* stacking interaction between the excited and ground state pyrene molecules, is very sensitive towards nitroaromatics. Recently, we and others used pyrene excimer fluorescence for the detection of nitroaromatic molecules utilizing nanomaterials that contain chemically attached or more simply physically encapsulated pyrene molecules.[14,24–32] However, most of these studies aimed to detect nitroaromatic explosives in the vapour phase or in organic solvents and studies for the determination of nitroaromatic explosive contaminated water are very rare.[26–29] In addition, for the materials with pyrene excimer emission, the detection limit in the aqueous phase is generally poor (at the μM level).[26–28] Herein, we demonstrated the trace (nM level) detection of TNT in the aqueous phase using pyrene confined mesostructured silica nanoparticles. In order to confine pyrene molecules in mesostructured silica nanoparticles, we firstly dissolved hydrophobic pyrene molecules in water using the cetyltrimethylammonium bromide (CTAB) surfactant. Pyrene molecules were encapsulated in the hydrophobic inner parts of the rod-shaped surfactant micelles.

[a]*UNAM-National Nanotechnology Research Center, Bilkent University, 06800 Ankara, Turkey. E-mail: bayindir@nano.org.tr*
[b]*Institute of Materials Science and Nanotechnology, Bilkent University, 06800 Ankara, Turkey*
[c]*Department of Physics, Bilkent University, 06800 Ankara, Turkey*
† Electronic supplementary information (ESI) available: Additional figures. See DOI: 10.1039/c4nr05514d

Then, we polymerized a silica precursor (tetraethyl orthosilicate, TEOS) around these micelles under basic conditions to obtain organic–inorganic hybrid nanoparticles that contain confined pyrene molecules inside their 2–3 nm sized MCM-41 type mesostructures. It is important to note that although similar surfactant assisted methods to load water-soluble dyes (*e.g.* R6G) into the pores of MCM-41 type MSNs have been reported,[33,34] in this study surfactant assisted loading of a water-insoluble molecule into the pores of MCM-41 type MSNs is reported, to our knowledge, for the first time. Nano-confinement of pyrene inside these mesostructures resulted in a bright and visible excimer emission. Recently, we reported that excimer emission of the pyrene doped materials can easily diminish in the course of time due to the dissociation of close proximity pyrene molecules.[24] To our surprise, we observed that pyrene excimer emission of these hybrid nanoparticles is stable for at least six months.

We studied the TNT sensing performance of the nanoparticles in water for the TNT concentration varying from 10 nM to 10 μM based on the quenching of excimer emission. We observed that the quenching of excimer emission is very selective and sensitive to TNT. In addition, emission quenching can be visually observed under UV-light enabling the naked-eye detection of TNT contaminated water. Pyrene confined mesostructured silica particles with their easy synthesis, high stability, high sensitivity and cost-effectiveness can be potentially used for the detection of TNT contaminated water.

Experimental section

Materials

Tetraethyl orthosilicate (TEOS), chloroform, and sodium hydroxide were purchased from Merck (Germany). Pluronic® F127, cetyltrimethylammoniumbromide (CTAB) and pyrene were purchased from Sigma-Aldrich (USA). All chemicals were used as received without any purification.

Synthesis of pyrene confined mesostructured silica nanoparticles

Pyrene confined mesostructured silica nanoparticles (pMSNs) were synthesized by slightly modifying the common MCM-41 type MSN synthesis methods.[35–39] Certain amounts of pyrene (6, 12, 22, and 40 mg) were dissolved in 500 μL of chloroform and 200 mg of CTAB was dissolved in 30 mL of deionized water. Then, pyrene solution was added to the CTAB solution and the mixture was stirred at 60 °C for 20 min. During stirring, chloroform evaporated and pyrene homogeneously dispersed in the CTAB solution. For the reaction mixture, 20 mg of F127 was dissolved in 66 mL of deionized water and 0.7 mL of 2.0 M sodium hydroxide solution was added. CTAB solution was added to the reaction mixture, and the mixture was heated to 80 °C. Then, 1 mL of TEOS was rapidly added under stirring at 600 rpm. The reaction mixture was refluxed for 2 h. Finally, the particles were collected by centrifugation at 9000 rpm for 20 min and washed with deionized water twice. Then, particles were dispersed in 80 mL of deionized water. The final particle concentration in the dispersion was 5.1 mg mL^{-1}.

Characterization of nanoparticles

The structure of pMSNs was investigated using a transmission electron microscope (TEM) (Tecnai G2-F30, FEI) and a scanning electron microscope (SEM) (Quanta 200 FEG, FEI). The absorption spectrum of pMSNs was recorded using a UV-Visible spectrophotometer (Cary 100, Varian). Fluorescence spectra of pMSNs were recorded using a fluorescence spectrophotometer (Cary Eclipse, Varian). Visual TNT detection experiments were performed using a UV inspection cabinet (Camag) with a UV lamp at 366 nm wavelength. Size distribution and the zeta potential of the nanoparticles were analysed using a zetasizer (Malvern Instruments).

Fluorescence quenching experiments

Fluorescence quenching based sensing experiments were performed in a quartz cuvette. 3 mL of 0.020 mg mL^{-1} pMSN dispersions were used for each sensing measurement. The fluorescence spectrum of pMSN dispersion was recorded before analyte addition (excitation wavelength was 340 nm). Then, TNT aqueous solutions were added in order to adjust the TNT concentrations between 10 nM and 10 μM and then, the fluorescence spectrum of the dispersion was recorded again. Selectivity experiments were performed using aqueous solutions of trinitrotoluene, dinitrotoluene, nitrobenzene, benzoic acid, aniline, chloroform, methanol, hydrochloric acid, sodium hydroxide, and sodium chloride. The final concentration of all interfering analytes was 10.0 μM in the fluorescence assay.

Results and discussion

pMSNs were synthesized *via* polymerization of the TEOS monomer in the presence of the CTAB surfactant under basic conditions. Basic conditions prevent the complete hydration of TEOS and increase the residual ethoxy groups to promote the self-assembly of negatively charged silicates with positively charged cetyltrimethylammonium (CTA) micelles.[40] Therefore, the ordered mesostructure was formed through the self-assembly of CTA micelles and silicates. Pyrene was added to the reaction mixture before the polymerization of silica and encapsulated by the hydrophobic parts of the CTA micelles (Fig. 1). Therefore, CTA micelles performed as both the templating agent for the formation of mesostructures and nanocontainers for pyrene confinement. In addition, we used a second surfactant (a pluronic block copolymer, F127) in order to prevent particle aggregation during the synthesis and to provide colloidal stability to the particles (Fig. 1).[41]

Fig. 2 shows TEM and SEM images of the pMSNs prepared using 40 mg of pyrene. pMSNs have mesostructures with sizes of approximately 2–3 nm. pMSNs are spherical in shape and their average particle size is 74 ± 9 nm (Fig. 2a). Also, the par-

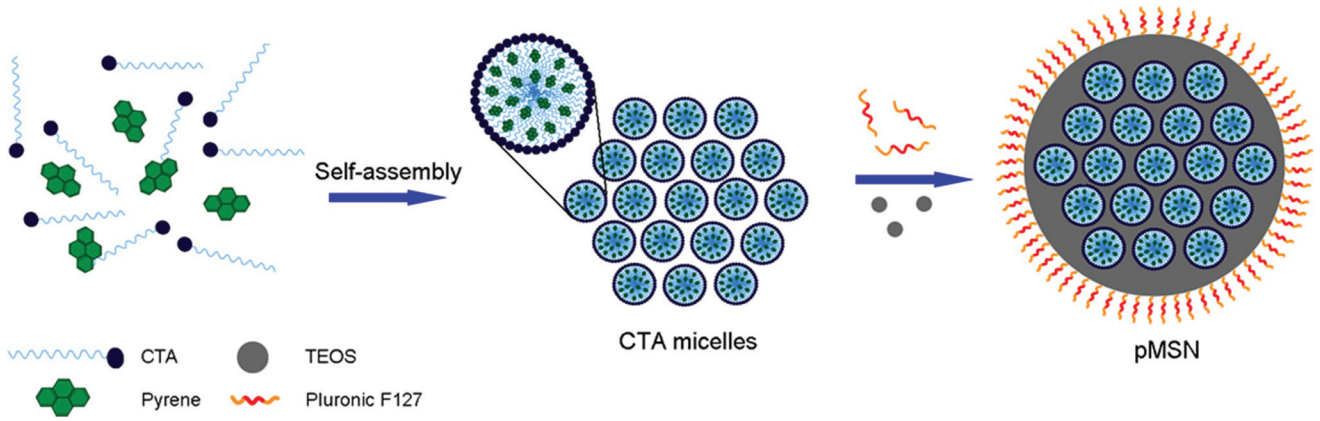

Fig. 1 Schematic representation for the formation of pMSNs. Pyrene is confined in CTA micelles through hydrophobic–hydrophobic interactions. After the addition of TEOS, silica grows around the self-assembled pyrene confined CTA micelles. F127 pluronic polymer prevents particle aggregation during the silica growth.

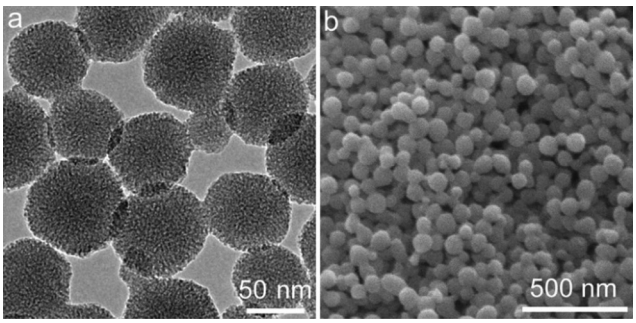

Fig. 2 Morphology of pMSNs. (a) TEM and (b) SEM images of the pMSNs prepared using 40 mg of pyrene indicating the uniform size and shape distribution of the nanoparticles.

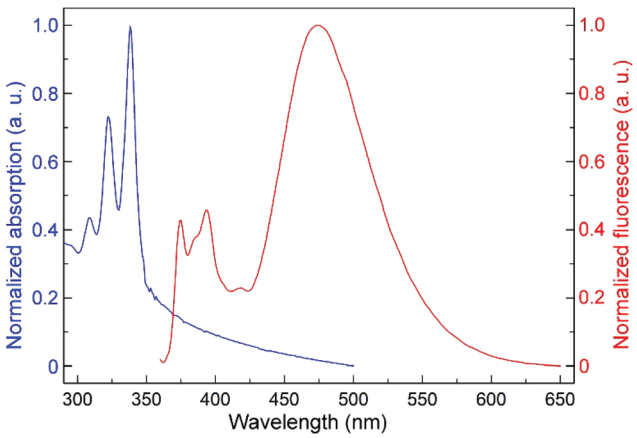

Fig. 3 UV-Visible absorption spectrum (blue) and fluorescence emission spectrum (red) (excitation wavelength was 340 nm) of pMSNs prepared using 40 mg of pyrene. Three peaks observed at 304, 321, and 336 nm are the absorption bands of pyrene. The peaks at 370–400 nm are the monomer emission of pyrene. The broad emission band centred at 475 nm is the excimer emission.

ticle size distribution of pMSNs is fairly narrow (Fig. 2b). In addition, we synthesized pMSNs using different amounts of pyrene: 6, 12, and 22 mg. We observed that the pyrene concentration significantly affects the size and shape of the silica nanoparticles. For instance, pMSNs prepared using 6 and 22 mg of pyrene have rod-like shapes with high polydispersity. Furthermore, pMSNs prepared using 12 mg of pyrene were interconnected during the synthesis which may cause poor colloidal stability in water (Fig. S1, ESI†).

Fig. 3 shows the UV-Visible absorption and fluorescence spectra of pMSNs prepared using 40 mg of pyrene. Three individual peaks at 304, 321, and 336 nm in the UV-Visible spectrum are the absorption bands of pyrene.[42] The emission bands around 370–400 nm in the fluorescence spectrum correspond to the monomer emission which is formed by the relaxation of the singlet excited pyrene.[42] The broad emission peak centred at 475 nm, on the other hand, is the excimer emission that occurs when an excited state pyrene makes the π–π^* stacking interaction with a ground state pyrene.[43] A high excimer emission intensity to monomer emission intensity (I_{exc}/I_{mon}) ratio (2.2) was observed for these nanoparticles (calculated using the intensities at 394 nm and 475 nm for the monomer and excimer emission, respectively). I_{exc}/I_{mon} ratios were determined to be 0.4, 0.8, and 1.8 for the pMSNs prepared using 6 mg, 12 mg, and 22 mg of pyrene, respectively (Fig. S2, ESI†). Since more pyrene molecules form more dimers through π-interaction, the excimer emission intensity and I_{exc}/I_{mon} ratios increased with increasing pyrene concentration. Accordingly, we used pMSNs prepared using 40 mg of pyrene in the rest of the study owing to their more uniformly distributed particle size and higher I_{exc}/I_{mon} ratio.

To determine the amount of pyrene that was encapsulated in pMSNs, we extracted pyrene using tetrahydrofuran (THF) and measured the absorption of the extracted pyrene using a UV-Visible absorption spectrophotometer. The pyrene content in the particles was calculated to be 0.038 mg mg^{-1} of pMSNs. Considering that the total amount of synthesized pMSNs was 410 mg, it can be calculated that almost 40% of pyrene used in the synthesis was encapsulated in the nanoparticles. Leakage of pyrene from CTA micelles of the mesostructured silica may

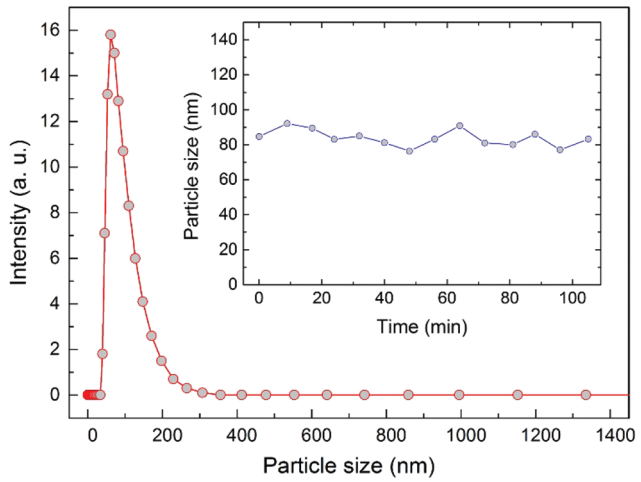

Fig. 4 Particle size distribution of the pMSNs measured using the dynamic light scattering technique. The inset shows the average particle size of pMSNs with respect to time.

cause decay of the excimer emission due to decreasing pyrene concentration in the pMSNs. To check the confinement stability of pyrene in the mesostructure, we centrifuged the pMSN dispersion (stored for six months under ambient conditions) and measured the emission of the supernatant. There was almost no emission signal in the supernatant indicating the stability of pyrene confined micelles inside the mesostructured silica nanoparticles (Fig. S3, ESI†). More importantly, after six months, pMSNs exhibited a bright excimer emission similar to that of the as-prepared particles (Fig. S4, ESI†). Also, the I_{exc}/I_{mon} ratio of the stored pMSNs was calculated to be 2.0 suggesting the long-term storability of these nanoparticles (inset in Fig. S4, ESI†).

The particle size distribution of pMSNs in water was determined using the dynamic light scattering (DLS) technique. The average particle size was measured to be 84.8 nm (Fig. 4), which is very close to the size calculated from the TEM images, indicating the good dispersibility of the nanoparticles in water. Furthermore, the zeta potential of the pMSNs was measured to characterize their surface charge. The surface of the pMSNs was found to be positively charged with a zeta potential of 33.8 mV which can be attributed to the positively charged CTA micelles. Besides dispersibility, colloidal stability of the nanoparticles is very important for reliable and repeatable fluorescence measurements. To investigate the stability of the particles, we measured the time-dependent size distribution of the pMSNs. The average particle size remained almost constant for at least 1.5 h which is far longer than the duration of a single sensing measurement (inset in Fig. 4).

pMSNs exhibit strong excimer emission in the absence of TNT molecules. When TNT binds to pyrene through the π–π* interaction, emission of pyrene is quenched through photo-induced electron transfer (PET) from an excited pyrene molecule to TNT.[23] To investigate the TNT sensing performance of the pMSNs, we recorded fluorescence spectra of pMSN dispersion before and after the addition of TNT with concentrations ranging from 10 nM to 10 μM. Both monomer and excimer emission intensities of pyrene were quenched gradually with increasing TNT concentration (Fig. 5a). After the addition of 10 μM of TNT, excimer emission was completely quenched, on the other hand, significant monomer emission still can be observed. Fig. 5b shows the rapid quenching of the excimer emission upon addition of 500 nM of TNT. Excimer emission quenching reaches its maximum within only 45 seconds and remains constant up to five minutes. It is important to note that in the absence of TNT, excimer emission is constant within the same time interval (Fig. 5b).

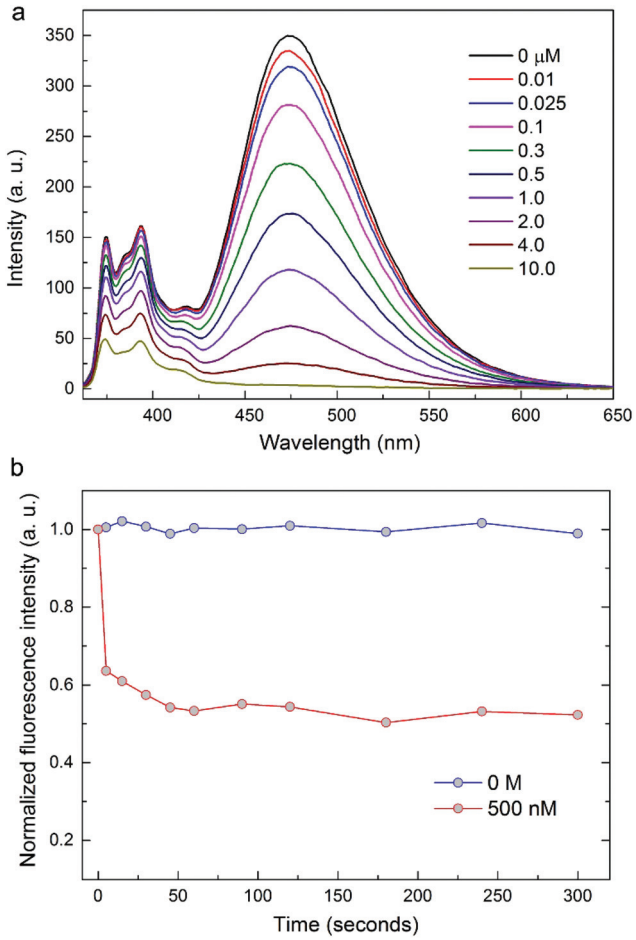

Fig. 5 (a) Fluorescence emission spectra of the pMSNs with increasing TNT concentrations. Excitation wavelength was set at 340 nm for the measurements. (b) Time-dependent excimer emission intensity of the pMSNs in the absence and in the presence of 500 nM of TNT.

Fig. 6a shows quenching efficiencies of the excimer and monomer emission of pMSNs depending on the TNT concentration. The quenching efficiency of the excimer emission at 475 nm was 3.1% for 10 nM of TNT and reached 67.2% and 98.9% when 1.0 μM and 10 μM of TNT were added, respectively. On the other hand, for all concentrations, the quenching efficiency of the monomer emission at 394 nm was lower than that of the excimer emission which indicates the higher sensitivity of the excimer emission against TNT (Fig. 6a). Fig. 6b shows the exponential fit to quenching data in the range from

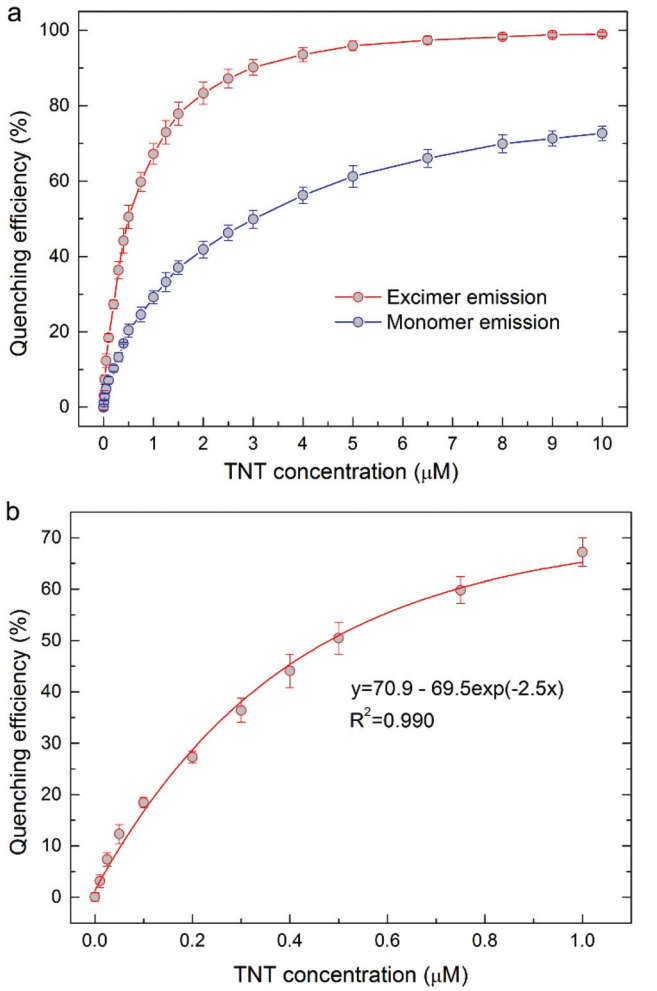

Fig. 6 (a) Quenching efficiencies of the pMSNs depending on the TNT concentration based on the excimer emission (at 475 nm) and monomer emission (at 394 nm). (b) Calibration curve for the TNT concentration in the range from 10 nM to 1.0 μM.

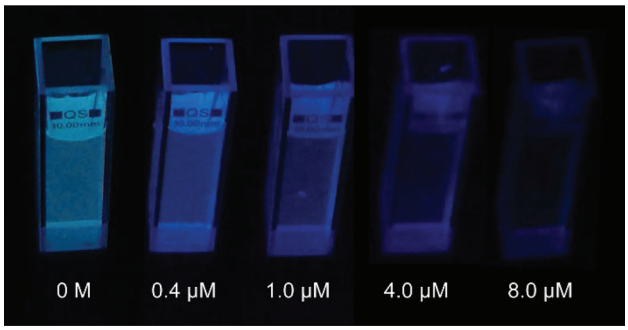

Fig. 7 Optical photographs of pMSN dispersions under UV-light before and after the addition of 0.4 μM, 1.0 μM, 4.0 μM, and 8.0 μM of TNT. Quenching of the excimer emission is clearly visible with the increasing TNT concentration.

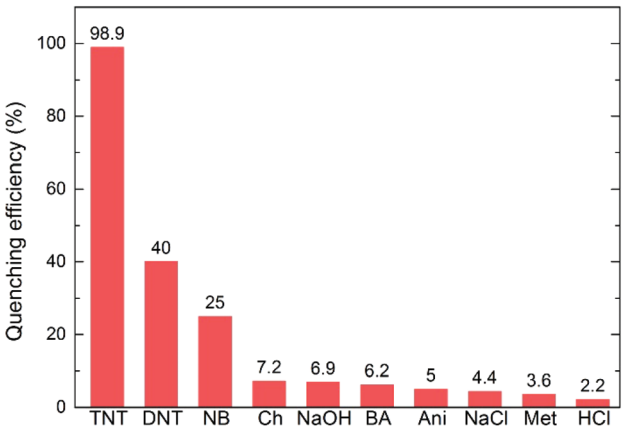

Fig. 8 Fluorescence quenching efficiencies of excimer emission for 10.0 μM aqueous solutions of various analytes (TNT: trinitrotoluene, DNT: dinitrotoluene, NB: nitrobenzene, Ch: chloroform, NaOH: sodium hydroxide, BA: benzoic acid, Ani: aniline, NaCl: sodium chloride, Met: methanol, and HCl: hydrochloric acid).

10 nM to 1.0 μM (regression constant is 0.990). Using this calibration curve, we calculated the practical detection limit of the fluorescent sensor to be 12 nM against TNT. According to the Environmental Protection Agency (EPA) report, the required detection threshold for TNT in tap water is approximately 10 nM. The calculated detection limit of pMSNs for TNT is very close to that reported by EPA suggesting the suitability of pMSNs for real-world applications.

In addition to the higher quenching efficiency of excimer emission, its bright blue colour enables the naked-eye detection of TNT. Accordingly, we performed visual detection experiments for 0.4 μM, 1.0 μM, 4.0 μM, and 8.0 μM of TNT under UV light (λ_{ex} = 366 nm) illumination. Excimer fluorescence of pMSN dispersion was very intense before the addition of TNT (Fig. 7). After the addition of 0.4 μM of TNT, which was found to quench the emission by 44.1% based on the fluorescence spectroscopy measurements, reduction in the emission intensity of pMSNs was visually observed under UV light. The emission intensity was further quenched with the increasing TNT concentration and almost no emission was observed under UV light with the addition of 8.0 μM of TNT (Fig. 7).

To demonstrate the selectivity of pMSNs against TNT, we measured the fluorescence of pMSNs after the addition of 10.0 μM aqueous solutions of various aromatic and non-aromatic substances. Fig. 8 shows the quenching efficiencies of excimer emission observed for the tested analytes. The quenching efficiency for TNT was 98.9% whereas quenching efficiencies for other nitroaromatic compounds were 40.0% and 25.0% for dinitrotoluene (DNT) and nitrobenzene (NB), respectively. On the other hand, chloroform, sodium hydroxide, benzoic acid, aniline, sodium chloride, methanol, and hydrochloric acid did not quench excimer emission significantly indicating the sensitivity of the excimer emission for nitroaromatic explosives. Lower quenching efficiencies for DNT and NB compared to that for TNT were due to their fewer nitro (NO_2) groups: DNT has two NO_2 groups and NB has one NO_2 group. Since the driving force for the electron transfer is

low reduction potential, TNT with its three NO_2 groups has the lowest reduction potential and higher electron accepting ability.[8,44] Therefore, excimer emission was quenched more in the presence of TNT compared to DNT and NB under the same conditions.

Conclusions

In this paper, we report a facile and low-cost method to prepare pyrene confined mesostructured silica nanoparticles (pMSNs) for sensitive detection of TNT in water. Pyrene was encapsulated in the mesostructured nanoparticles through hydrophobic–hydrophobic interactions between the templating agent CTA micelles and pyrene molecules during the particle growth. The resulting spherical organic–inorganic hybrid nanoparticles have fairly uniform size distribution and good colloidal stability in water. More importantly, bright and visible pyrene excimer emission was observed for pMSNs which is stable for at least six months. Excimer emission of the pMSNs exhibits a rapid quenching against TNT. A practical detection limit of 12 nM was achieved for TNT in water which is very close to the maximum allowable concentration of TNT (determined by EPA) in tap water (10 nM). Nevertheless, further studies may be needed to improve the sensitivity of the proposed method and make it more suitable for real-world applications. Furthermore, quenching of the excimer emission is visually observed under UV-light suggesting the naked-eye detection of TNT at the submicromolar level. In addition, excimer emission quenching of pMSNs shows a high selectivity for TNT. We believe that our pyrene confined mesostructured silica nanoparticles hold a significant potential for rapid and reliable detection of nitro-explosive contaminated water with their simple synthesis, sensitivity, and selectivity.

Acknowledgements

We would like to thank Tamer Dogan for his help with visual detection experiments and Mustafa Guler for the TEM images. This work is supported by TÜBİTAK under the Project No. 111T696. M.B. acknowledges partial support from the Turkish Academy of Sciences (TUBA).

Notes and references

1 J. Hawari, S. Beaudet, A. Halasz, S. Thiboutot and G. Ampleman, Microbial degradation of explosives: biotransformation versus mineralization, *Appl. Microbiol. Biotechnol.*, 2000, **54**, 605–618.
2 N. Hannink, S. J. Rosser, C. E. French, A. Basran, J. A. H. Murray, S. Nicklin and N. C. Bruce, Phytodetoxification of TNT by transgenic plants expressing a bacterial nitroreductase, *Nat. Biotechnol.*, 2001, **19**, 1168–1172.
3 M. E. Germain and M. J. Knapp, Optical explosives detection: from color changes to fluorescence turn-on, *Chem. Soc. Rev.*, 2009, **38**, 2543–2555.
4 Y. Salinas, R. Martínez-Máñez, M. D. Marcos, F. Sancenón, A. M. Costero, M. Parra and S. Gil, Optical chemosensors and reagents to detect explosives, *Chem. Soc. Rev.*, 2012, **41**, 1261–1296.
5 S. Singh, Sensors-An effective approach for the detection of explosives, *J. Hazard. Mater.*, 2007, **144**, 15–28.
6 J. S. Caygill, F. Davis and S. P. J. Higson, Current trends in explosive detection techniques, *Talanta*, 2012, **88**, 14–29.
7 D. S. Moore, Instrumentation for trace detection of high explosives, *Rev. Sci. Instrum.*, 2004, **75**, 2499–2512.
8 S. J. Toal and W. C. Trogler, Polymer sensors for nitroaromatic explosives detection, *J. Mater. Chem.*, 2006, **16**, 2871–2883.
9 K. Zhang, H. Zhou, Q. Mei, S. Wang, G. Guan, R. Liu, J. Zhang and Z. Zhang, Instant Visual Detection of Trinitrotoluene Particulates on Various Surfaces by Ratiometric Fluorescence of Dual-Emission Quantum Dots Hybrid, *J. Am. Chem. Soc.*, 2011, **133**, 8424–8427.
10 R. Freeman, T. Finder, L. Bahshi, R. Gill and I. Willner, Functionalized CdSe/ZnS QDs for the Detection of Nitroaromatic or RDX Explosives, *Adv. Mater.*, 2012, **24**, 6416–6421.
11 S. Xu, H. Lu, J. Li, X. Song, A. Wang, L. Chen and S. Han, Dummy Molecularly Imprinted Polymers-Capped CdTe Quantum Dots for the Fluorescent Sensing of 2,4,6-Trinitrotoluene, *ACS Appl. Mater. Interfaces*, 2013, **5**, 8146–8154.
12 D. Li, J. Liu, R. T. K. Kwok, Z. Liang, B. Z. Tang and J. Yu, Supersensitive detection of explosives by recyclable AIE luminogen-functionalized mesoporous materials, *Chem. Commun.*, 2012, **48**, 7167–7169.
13 A. Rana and P. K. Panda, Fluorescent turn-off based sensing of nitrated explosives using porphyrins and their Zn(II)-derivatives, *RSC Adv.*, 2012, **2**, 12164–12168.
14 S. Shanmugaraju, S. A. Joshi and P. S. Mukherjee, Fluorescence and visual sensing of nitroaromatic explosives using electron rich discrete fluorophores, *J. Mater. Chem.*, 2011, **21**, 9130–9138.
15 H. Li, Y. Zhu, J. Zhang, Z. Chi, L. Chen and C.-Y. Su, Luminescent metal–organic gels with tetraphenylethylene moieties: porosity and aggregation-induced emission, *RSC Adv.*, 2013, **3**, 16340–16344.
16 B. Gole, A. K. Bar and P. S. Mukherjee, Fluorescent metal–organic framework for selective sensing of nitroaromatic explosives, *Chem. Commun.*, 2011, **47**, 12137–12139.
17 Y.-N. Gong, L. Jiang and T.-B. Lu, A highly stable dynamic fluorescent metal–organic framework for selective sensing of nitroaromatic explosives, *Chem. Commun.*, 2013, **49**, 11113–11115.
18 D. T. McQuade, A. E. Pullen and T. M. Swager, Conjugated Polymer-Based Chemical Sensors, *Chem. Rev.*, 2000, **100**, 2537–2574.

19 A. Rose, Z. Zhu, C. F. Madigan, T. M. Swager and V. Bulovic, Sensitivity gains in chemosensing by lasing action in organic polymers, *Nature*, 2005, **434**, 876–879.
20 L. Feng, H. Li, Y. Qu and C. Lu, Detection of TNT based on conjugated polymer encapsulated in mesoporous silica nanoparticles through FRET, *Chem. Commun.*, 2012, **48**, 4633–4635.
21 Y. Z. Liao, V. Strong, Y. Wang, X.-G. Li, X. Wang and R. B. Kaner, Oligotriphenylene Nanofiber Sensors for Detection of Nitro-Based Explosives, *Adv. Funct. Mater.*, 2012, **22**, 726–735.
22 T. M. Figueira-Duarte and K. Mullen, Pyrene-Based Materials for Organic Electronics, *Chem. Rev.*, 2011, **111**, 7260–7314.
23 Y. Wang, A. La, Y. Ding, Y. Liu and Y. Lei, Novel Signal-Amplifying Fluorescent Nanofibers for Naked-Eye-Based Ultrasensitive Detection of Buried Explosives and Explosive Vapors, *Adv. Funct. Mater.*, 2012, **22**, 3547–3555.
24 P. Beyazkilic, A. Yildirim and M. Bayindir, Formation of Pyrene Excimers in Mesoporous Ormosil Thin Films for Visual Detection of Nitro-explosives, *ACS Appl. Mater. Interfaces*, 2014, **6**, 4997–5004.
25 G. B. Demirel, B. Daglar and M. Bayindir, Extremely fast and highly selective detection of nitroaromatic explosive vapours using fluorescent polymer thin films, *Chem. Commun.*, 2013, **49**, 6140–6142.
26 H. Du, G. He, T. Liu, L. Ding and Y. Fang, Preparation of pyrene-functionalized fluorescent film with a benzene ring in spacer and sensitive detection to picric acid in aqueous phase, *J. Photochem. Photobiol., A*, 2011, **217**, 356–362.
27 T. Liu, L. Ding, K. Zhao, W. Wang and Y. Fang, Single-layer assembly of pyrene end-capped terthiophene and its sensing performances to nitroaromatic explosives, *J. Mater. Chem.*, 2012, **22**, 1069–1077.
28 G. He, N. Yan, J. Yang, H. Wang, L. Ding, S. Yin and Y. Fang, Pyrene-Containing Conjugated Polymer-Based Fluorescent Films for Highly Sensitive and Selective Sensing of TNT in Aqueous Medium, *Macromolecules*, 2011, **44**, 4759–4766.
29 Y. Wang, A. La, C. Bruckner and Y. Lei, FRET- and PET-based sensing in a single material: expanding the dynamic range of an ultra-sensitive nitroaromatic explosives assay, *Chem. Commun.*, 2012, **48**, 9903–9905.
30 A. Vu, J. Phillips, P. Bühlmann and A. Stein, Quenching Performance of Surfactant-Containing and Surfactant-Free Fluorophore-Doped Mesoporous Silica Films for Nitroaromatic Compound Detection, *Chem. Mater.*, 2013, **25**, 711–722.
31 K. Sarkar, Y. Salinas, I. Campos, R. Martínez-Máñez, M. D. Marcos, F. Sancenón and P. Amorós, Organic–Inorganic Hybrid Mesoporous Materials as Regenerable Sensing Systems for the Recognition of Nitroaromatic Explosives, *ChemPlusChem*, 2013, **78**, 684–694.
32 W. Chen, N. B. Zuckerman, J. P. Konopelski and S. Chen, Pyrene-Functionalized Ruthenium Nanoparticles as Effective Chemosensors for Nitroaromatic Derivatives, *Anal. Chem.*, 2010, **82**, 461–465.
33 E.-B. Cho, D. O. Volkov and I. Sokolov, Ultrabright Fluorescent Silica Mesoporous Silica Nanoparticles: Control of Particle Size and Dye Loading, *Adv. Funct. Mater.*, 2011, **21**, 3129–3135.
34 S. Palantavida, R. Tang, G. P. Sudlow, W. J. Akers, S. Achilefu and I. Sokolov, Ultrabright NIR Fluorescent Mesoporous Silica Nanoparticles, *J. Mater. Chem. B*, 2014, **2**, 3107–3114.
35 C. T. Kresge, M. E. Leonowicz, W. J. Roth, J. C. Vartuli and J. S. Beck, Ordered Mesoporous Molecular Sieves Synthesized by A Liquid-crystal Template Mechanism, *Nature*, 1992, **359**, 710–712.
36 J. S. Beck, J. C. Vartuli, W. J. Roth, M. E. Leonowicz, C. T. Kresge, K. D. Schmitt, C. T. W. Chu, D. H. Olson, E. W. Sheppard, S. B. McCullen, J. B. Higgins and J. L. Schlenker, A New Family of Mesoporous Molecular Sieves Prepared with Liquid Crystal Templates, *J. Am. Chem. Soc.*, 1992, **114**, 10834–10843.
37 Q. Cai, Z. S. Luo, W. Q. Pang, Y. W. Fan, X. H. Chen and F. Z. Cui, Dilute Solution Routes to Various Controllable Morphologies of MCM-41 Silica with a Basic Medium, *Chem. Mater.*, 2001, **13**, 258–263.
38 M. Liong, J. Lu, M. Kovochich, T. Xia, S. G. Ruehm, A. E. Nel, F. Tamanoi and J. I. Zink, Multifunctional Inorganic Nanoparticles for Imaging, Targeting, and Drug Delivery, *ACS Nano*, 2008, **2**, 889–896.
39 A. Yildirim, H. Budunoglu, B. Daglar, H. Deniz and M. Bayindir, One-Pot Preparation of Fluorinated Mesoporous Silica Nanoparticles for Liquid Marble Formation and Superhydrophobic Surfaces, *ACS Appl. Mater. Interfaces*, 2011, **3**, 1804–1808.
40 K. Suzuki, K. Ikari and H. Imai, Synthesis of Silica Nanoparticles Having a Well-Ordered Mesostructure Using a Double Surfactant System, *J. Am. Chem. Soc.*, 2004, **126**, 462–463.
41 S. Febvay, D. M. Marini, A. M. Belcher and D. E. Clapham, Targeted Cytosolic Delivery of Cell-Impermeable Compounds by Nanoparticle-Mediated, Light-Triggered Endosome Disruption, *Nano Lett.*, 2010, **10**, 2211–2219.
42 F. M. Winnik, Photophysics of Preassociated Pyrenes in Aqueous Polymer Solutions and in Other Organized Media, *Chem. Rev.*, 1993, **93**, 587–614.
43 J. B. Birks, Excimers, *Rep. Prog. Phys.*, 1975, **38**, 903–974.
44 J. S. Yang and T. M. Swager, Fluorescent Porous Polymer Films as TNT Chemosensors: Electronic and Structural Effects, *J. Am. Chem. Soc.*, 1998, **120**, 11864–11873.